Secondary Organic Aerosol Formation from Limonene Ozonolysis: Homogeneous and Heterogeneous Influences as a Function of NO_x

Jieyuan Zhang, Kara E. Huff Hartz, Spyros N. Pandis, and Neil M. Donahue*

Center for Atmospheric Particle Studies, Carnegie Mellon University, 500 Forbes Avenue, Pittsburgh, Pennsylvania 15213

Received: May 9, 2006; In Final Form: August 2, 2006

Limonene has a high emission rate both from biogenic sources and from household solvents. Here we examine the limonene + ozone reaction as a source for secondary organic aerosol (SOA). Our data show that limonene has very high potential to form SOA and that NO_x levels, O_3 levels, and UV radiation all influence SOA formation. High SOA formation is observed under conditions where both double bonds in limonene are oxidized, but those conditions depend strongly on NO_x. At low NO_x, heterogeneous oxidation of the terminal double bond follows the initial limonene ozonolysis (at the endocyclic double bond) almost immediately, making the initial reaction rate limiting. This requires a high uptake coefficient between ozone and the first-generation, unsaturated organic particles. However, at high NO_x, this heterogeneous processing is inhibited and gas-phase oxidation of the terminal double bond dominates. Although this chemistry is slower, it also yields products with low volatility. UV light suppresses production of the lowest volatility products, as we have shown in earlier studies of the α-pinene + ozone reaction.

1. Introduction

Limonene is an important member in the monoterpene family (Figure 1). It has a high biogenic source[1−4] and it is also important indoors[5−9] as a common "green" solvent. Although the emission rate of limonene is less than that of α-pinene, limonene has a much higher potential for secondary organic aerosol (SOA) formation because it is doubly unsaturated.[3,10] Although some products have been identified in limonene ozonolysis,[10−13] the SOA formation from the reaction of limonene and ozone has not been studied systematically over the range of conditions found in the atmosphere.

Recent consideration of SOA chemistry has emphasized multigeneration oxidation (aging) on SOA formation.[14−17] Moreover, once reaction products have sufficiently low vapor pressures to be found significantly in both the vapor and condensed phases, aging can occur in either phase.[18,19] Condensed-phase aging chemistry is additionally interesting because there is considerable evidence that heterogeneous uptake coefficients measured for simple systems in the laboratory may be very different from the uptake coefficients on real atmospheric particles;[19,20] the cause of these changes in uptake coefficients is an area of very active research.[20−22] Limonene is thus an excellent model system for multi-generation SOA formation: it is important in the atmosphere, it has two double bonds with very different ozonolysis rate constants, the first-generation products should partition significantly into the condensed phase, and the second generation products-should have still lower vapor pressures.

From the point of view of SOA formation, we need to know the distribution of vapor pressures of the reaction products, even if we cannot identify them all. Our broad objective is to understand how the volatility distribution of limonene oxidation products evolves through two generations of oxidation, what steps are rate-limiting in this process, what effects common in the atmosphere may change this product volatility distribution, and finally what phase various reactions occur in. We shall interpret our findings in the context of a "volatility basis set",[15] finding a set of product mass yields $\{\alpha\}$ spanning a basis set of saturation mass concentrations $\{C^*\}$ under a number of conditions and then assessing these findings in terms of known gas- and condensed-phase chemistry.

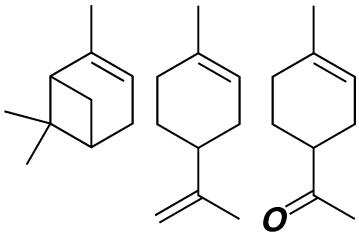

Figure 1. Three terpenes discussed in this paper: α-pinene, limonene, and limonoketone.

We shall address this complex system in a series of papers. The subject here is the chemistry of this process and how that chemistry changes under different conditions, with added insight from our theoretical work on organic nitrate formation.[23] In another paper, we describe SOA formation from limonoketone,[24] which effectively "preselects" one (higher volatility) pathway for the second (exo) ozonolysis step in limonene and allows us to directly test the hypothesis that the initial ozonolysis step in limonene + ozone should resemble α-pinene + ozone in terms of SOA formation. Finally, we address the system from the perspective of the temperature dependence of overall SOA formation, constraining the SOA formation potential of limonene and its overall implications to air quality.[25]

2. Background

2.1. Terpene Ozonolysis. Limonene has two very different double bonds—an endo- trisubstituted double bond and an exo-

* To whom correspondence should be addressed. E-mail: nmd@andrew.cmu.edu.

10.1021/jp062836f CCC: $33.50
Published on Web 09/07/2006

terminal bisubstituted double bond. When limonene reacts with O_3, it follows the "Criegee Mechanism",[26] forming at least four sets of carbonyl-oxide Criegee Intermediates (CI) and carbonyl products.[10] Each CI may then undergo a series of unimolecular reactions, ultimately forming various peroxy radicals after the addition of O_2 to some resulting fragments. There are ample opportunities for gas-phase chemistry to alter the final product distribution and thus SOA production. Furthermore, oxidation of the endocyclic double bond alone leads to formation of organic aerosol and, thus, unsaturated condensed-phase compounds. These in turn may be oxidized by heterogeneous pathways; we shall present evidence in this paper that heterogeneous oxidation may dominate this second oxidation step.

The rate constant for the limonene + ozone reaction is 2×10^{-16} cm^3 molecule^{-1} s^{-1},[27,28] but the specific addition of O_3 to each double bond has not been studied directly. The reference data for homologous alkene + O_3 reactions[29−32] show that the rate constant of O_3 addition to the carbon−carbon double bond increases with increasing number and size of the substitution group connected to the two α carbon atoms, with the rate constant increasing by a factor of 10 for each CH_3 group added. Symmetry matters as well—substituents on either side of the double bond are more important than those on the same side, and terminal double bonds have slow ozonolysis rate constants. Also, the reaction between O_3 and limonene aldehyde, which has only one exo- terminal carbon−carbon double bond, has an ozonolysis rate constant of 8×10^{-18} cm^3 molecule^{-1} s^{-1}.[12] The evidence strongly suggests that the endo- double bond of limonene has a specific addition rate constant a factor of 10−50 faster than the exo- double bond.

2.2. Semivolatile Partitioning. Oxidation of large hydrocarbons produces a rich set of reaction products, even for relatively simple model systems. Even though we may not know the complete product distribution, nor the appropriate activity coefficients for the resulting condensed-phase mixture, we need to constrain the volatility distribution of the reaction products. The accepted procedure is to measure the ratio of aerosol mass formed to precursor (terpene) mass reacted, which we call the aerosol mass fraction (AMF, ξ). This is measured over a wide range of total aerosol mass concentrations C_{OA}, which influences the semi-volatile partitioning; only low-volatility material condenses at low total C_{OA}, whereas higher-volatility material can condense as well at high C_{OA}.

The volatility of a compound is given by a saturation mass concentration, C^*, which incorporates the vapor pressure but also activity coefficients of the material. A C_{OA} of 1 μg m^{-3} is typical of the remote atmosphere, and under those conditions, a compound with $C^* = 1$ μg m^{-3} will be evenly split between the condensed and vapor phases. For a mid-sized organic compound ($M = 280$ g mole^{-1}), 1 μg m^{-3} is equivalent to 100 pptv or a vapor pressure of 10^{-7} mb. Vapor pressures this low are extremely difficult to measure directly.

The seminal treatment of Pankow[33,34] was extended to SOA in the form of a "2-product model" by Odum,[35] where two surrogate products are used to parameterize data with a pair of yields α_i and saturation concentrations C_i^*. We have recently[15] expanded this formalism by considering a basis set of saturation concentrations $\{C^*\}$ at fixed values spanning the full range of C_{OA} observed in the atmosphere, separated by powers of 10. We are thus able to fit SOA formation data over a wide range, constraining the product volatility distribution even for an unknown set of products, for example, with α-pinene.[36]

A major advantage of the basis-set formalism is that all semivolatiles can be treated uniformly. This includes primary organic aerosol emissions, which are semi-volatile,[37] and it also allows us to frame the question of what multiple generations of oxidation will do to the volatility distribution. We expect semivolatile organic compounds in the atmosphere to undergo many generations of oxidation, probably 7 or more.[14] Over much of this range, oxidation is likely to move the volatility distribution primarily toward lower volatility. In the atmosphere, this aging may be accomplished by any oxidant, but it is likely that OH radicals will play a major role. Non-oxidative chemistry may also be important, for example, in the formation of macromolecules.[38]

Although the volatility basis set is a practical construct designed to aid atmospheric modeling, it also provides an important tool for fundamental studies focusing on the underlying chemistry; once we concede that we are unlikely to completely describe to composition of SOA particles, the volatility distribution of the reaction products becomes a bulk property that can significantly aid fundamental interpretations.

2.3. NO_x and UV Effects. The presence of NO_x (NO and NO_2) can dramatically change gas-phase organic oxidation mechanisms. The NO_x concentration is typically 10−1000 ppbv in urban and suburban areas[39−41] but as low as 10 ppt in very remote areas.[42] NO_x levels are important to SOA formation for both biogenic and anthropogenic compounds,[43−45] primarily because NO_x intercepts the atmospheric chemical mechanism involving organo-peroxy radicals (RO_2). In high-NO_x areas, nitrate can be an important component of fine particles, comprising up to one-third of the aerosol mass.[39,46−48] Inorganic nitrate (nitric acid) is the dominant condensed-phase form, but organic nitrates have been observed in atmospheric particles as well. Zhang et al.[23] developed an organic nitrate yield model for peroxy radicals reacting with NO, using quantum chemistry and statistical reaction dynamics to extend experimental results and empirical models[49,50] to large carbon numbers and high pressures. For secondary peroxy radicals with 10 carbon atoms in the molecule, the nitrate yield at 760 Torr and 298 K is around 0.4. There are 9 or 10 carbon atoms in the peroxy radicals that formed from limonene ozonolysis in the presence of O_2. Consequently, the nitrate formation from the reaction of large peroxy radicals and NO is substantial, and the influence of the nitrate products on SOA formation needs to be considered for a complete picture of the SOA formation from limonene and ozone reaction.

Recently, Presto et al. addressed the effects of NO_x and UV radiation on α-pinene ozonolysis.[36,45] The overall conclusion of these studies is that high NO_x and UV radiation both decrease SOA formation from α-pinene. The presumed reason for the NO_x effect is that it will compete with HO_2 for the peroxy radicals formed from α-pinene ozonolysis in the presence of O_2. Furthermore, the organic nitrate and carbonyl products from the NO_x pathway are more volatile than the acid products from the HO_2 pathway. UV radiation may enhance the decomposition of some products, especially in the low-NO_x pathway, forming the less volatile carbonyl products.

Here, we shall explore this chemistry for limonene ozonolysis. As we shall show, the NO_x effect really consists of two competing effects. Evidently high-NO_x products are more volatile than their low-NO_x counterparts; however, NO_x can also add mass to SOA, so under conditions where SOA will be formed in any event, the nitrates will be more massive and thus SOA formation can increase, on a mass basis. Under different circumstances, one effect or the other can dominate for limonene, making this an interesting system.

3. Experimental Methods

3.1. Smog Chamber. Experiments were conducted in an environmental chamber consisting of a 10 m^3 Teflon bag (Welch Fluorocarbon) suspended inside a temperature-controlled room held at 25 ± 2 °C and 2−10% RH.[36,45,51,52] Before each experiment, the bag was cleaned by injecting 1 ppm of O_3 with UV illumination at 40 °C. We then purged the illuminated bag with filtered air (particle filter, hydrocarbon filter, and silica gel filter) for more than 2 h. At the end of this cycle, the particle count in the chamber was less than 2 particles cm^{-3}.

For most experiments, 0.2 mL 2-butanol (99.5%, Aldrich) was injected into the bag to scavenge OH produced in the ozonolysis.[53] The roughly 5 ppm of 2-butanol forced the HO_x balance from OH toward HO_2. Ultimate HO_x loss in the chamber is through HO_2 and the formation of peroxides under low-NO_x conditions[54] and through inorganic nitrate formation under high-NO_x conditions. The butanol forced the RO_2 chemistry in the chamber to follow the desired pathways in addition to preventing OH from reacting with limonene.

For high-NO_x experiments, 1% NO in nitrogen was injected to reach the desired NO_x concentration. The "low-NO_x" experiments had ambient NO_x levels. Both NO and NO_2 concentrations were monitored by a NO_x monitor (API, 200A). O_3 was added to the bag by passing pure oxygen gas through an ozone generator (Azcozon, HTU500AC), and its concentration was monitored by an ozone monitor (Dasibi, 1008-PC). Because O_3 will oxidize NO to NO_2 quickly, and NO plays the most important role in the experiments, UV lights (three banks of UV lights, General Electric model 10526 black lights) were kept on in all of the high-NO_x experiments and some of the low-NO_x experiments.

After the concentrations of O_3 and NO_x reached the desired values, a mixture of R-(+)-limonene (99+%, Aldrich) and *n*-pentane (99+%, Aldrich) was injected into the bag. When the mixing was complete, which usually took 180−300 s, all the input flows to the smog chamber were shut off and the experiment commenced.

The gas-phase hydocarbons were monitored by both a gas chromatograph with flame ionization detector (GC-FID, Perkin-Elmer AutoSystem XL; J&W Scientific DB-624 capillary column, 30 m × 0.530 mm) and a proton-transfer reaction mass spectrometer (Ionocon PTR-MS). Limonene was measured by both GC-FID and PTR-MS at $m/z = 137$ and 81. The particle size distribution inside the chamber was monitored by both a scanning mobility particle sizer (TSI, 3936) and an aerodyne electron impact ionization quadrupole aerosol mass spectrometer (Aerodyne Q-AMS).

The AMS was also used to detect the size distribution of the fragments in the aerosol including mass 30 (NO^+) and 46 (NO_2^+), which are associated with organic nitrates. A few experiments were carried out in a 100 L Teflon bag with synthetic air to obtain AMS spectra for rigorously NO_x-free conditions, where minor organic fragments at $m/z = 30$ and 46 could be measured.

4. Results

The normalized aerosol mass fraction (ξ') is the ratio of the mass concentration of the aerosol formed to the mass concentration of the VOC reacted, assuming a particle density of 1 g cm^{-3}. The AMF reflects both chemical product yields and semivolatile partitioning.[15] We focus on aerosol mass, rather than molar yields, both because our measurements are mass (or volume) based and because particulate mass is of regulatory interest—the EPA $PM_{2.5}$ standard is based on total mass. Our standard aerosol measurement is of volume with the SMPS; because the particle density is unknown, we strongly advocate the use of the normalized AMF to facilitate the intercomparison of experimental results without ambiguities associated with assumed density. Although density can be determined by combining the AMS and SPMS data, we are not yet sufficiently confident in these values to rely on them here.

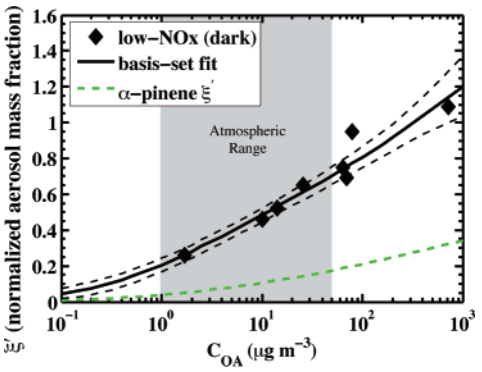

Figure 2. Aerosol mass fraction vs C_{OA} for low-NO_x experiments, including a basis-set fit shown as a black curve with a dashed confidence interval. For comparison, the fit for α-pinene under similar circumstances is shown as a dashed green line.

For most of the experiments reported here, gas-phase precursor oxidation was rapid and particle nucleation and condensation of saturated vapors was also rapid compared with particle wall loss. Under these conditions, the mass balance for wall loss is straightforward but essential.[36] The experiments were conducted with high ozone (>700 ppbv) to ensure rapid oxidation of both double bonds and also to reduce the effect of vapor wall losses at low condentrations.[55] Where secondary chemistry is an issue, one must consider the possibility of continued particle growth due to secondary chemistry, so we typically do wall loss calculations based both on particle volume and particle number; volume is insensitive to coagulation but number is insensitive to continued growth. For the data reported here, both corrections agree within error.

We conducted experiments under five different sets of conditions: high-NO_x with and without 2-butanol (with UV); low-NO_x with and without UV radiation (with 2-butanol); and zero-NO_x (with 2-butanol) in the 100 L Teflon bag. The results are tabulated in the Supporting Information. High-NO_x is defined as VOC:$NO_x \leq 1$ (ppbC/ppb), whereas low-NO_x is defined as the VOC:NO_x ratio $\geq$ 10 (ppbC/ppb). In several low-NO_x experiments, the limonene concentrations were very low, so the VOC:NO_x was between 1 and 10 (ppbC/ppb) even though no additional NO was added to the bag. We classify these experiments as low-NO_x.

The NO_x divisions are based on a crude measure of RO_2 branching, defined as β:[45]

$$\beta = \text{VOC:NO}_x/10 = [\text{limonene}]/[\text{NO}_x] \qquad (1)$$

This roughly defines the fraction of RO_2 reacting with NO_x as opposed to HO_2, though the real branching certainly evolves during the experiments. Our interest is in the limiting cases, so our analysis will focus entirely on the low- and high-NO_x data; as we have shown for α-pinene,[56] the intermediate-NO_x results can be described by a linear combination of low- and high-NO_x product yields based on RO_2 branching.

4.1. Base Case: Low-NO_x, High-O_3. The standard condition for these and other SOA experiments is low-NO_x ozonolysis with butanol. Our results are shown in Figure 2, along with the partitioning curve for α-pinene[56] and a basis-set fit for limonene.

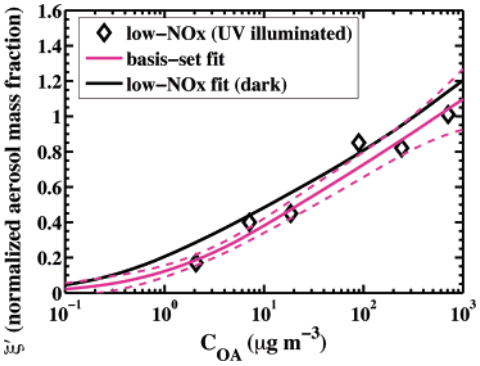

Figure 3. Suppression of low-NO_x SOA formation under UV illumination (◊). The fit (magenta curve) is consistent with a reduction of a factor of 2 (0.15) in the yield of 1 μg m^{-3} material from the dark experiments (shown with a black curve).

SOA formation from limonene + O_3 is dramatically larger than for α-pinene over the full atmospheric range of C_{OA}. By themselves, these data provide strong evidence that the limonene is fully oxidized. They also show that limonene is an important SOA source; on a mass basis, it is 4−5 times more effective at SOA formation than α-pinene.

The mass yields in the basis-set fit are {0, 0.03, 0.29, 0.31, 0.30, 0.60} for vapor pressures ranging from 0.01 to 1000 μg m^{-3}.[15,56] The 0.01 μg m^{-3} yield is set to zero because it is not constrained by the data. Individual parameter uncertainties are meaningless due to covariance; however, the overall uncertainty in the fit is of order 10% plus an absolute error of approximately 0.02, as shown by the dashed 95% confidence interval.

4.2. UV Radiation Effect. Under low-NO_x conditions, SOA from α-pinene + ozone was sharply reduced with UV illumination.[36] The reduction appears in a basis-set fit in the volatility bin centered at $C^* = 1$ μg m^{-3}, with the mass yield changing from 0.05 in the dark to 0.02 under UV illumination,[56] consistent with a loss due to photolysis of about 60% of the material at that volatility. There was no sign of the material appearing in more volatile bins. This translates into a factor of 2 reduction of the overall AMF values in the atmospherically relevant concentration range for α-pinene + ozone.

We observed a similar effect for limonene, illustrated in Figure 3. The mass yields in the basis-set fit are {0, 0.006, 0.15, 0.40, 0.31, 0.50}, so again the major effect is that the mass yield in the 1 μg m^{-3} bin is reduced by a factor of 2 (0.29 to 0.15). The effected material could easily have a volatility lower than 1 μg m^{-3}, as our data do not extend to such low C_{OA}. There is minor rearrangement in the higher volatility bins that is not statistically significant—the curve itself is essentially parallel to the dark curve (shown in black in Figure 3).

Though the change is marginally significant statistically, individual data points are consistently lower under UV illumination, and the fractional drop in AMF over the atmospheric range is quite large. As with α-pinene, the UV effect is only seen during the aerosol growth stage (figures in the Supporting Information); this suggests either that a gas-phase intermediate is photolized during the active chemistry phase or that a terminal product is only lost from the vapor phase due to condensed-phase quenching of the photolysis. Because we have never seen late-stage photolysis, even under conditions where we would expect the photolabile product to be partially vaporized, we conclude that the photolysis most likely involves a reactive intermediate.

4.3. NO_x Concentration Effect at High O_3. SOA formation from α-pinene + ozone drops dramatically under high-NO_x conditions.[45] Our high-NO_x results are shown in Figure 4 with data and a basis-set fit shown in red giving yields of {0, 0.02, 0.21, 0.44, 0.40, 0.87}. The dark, low-NO_x result is again shown in black.

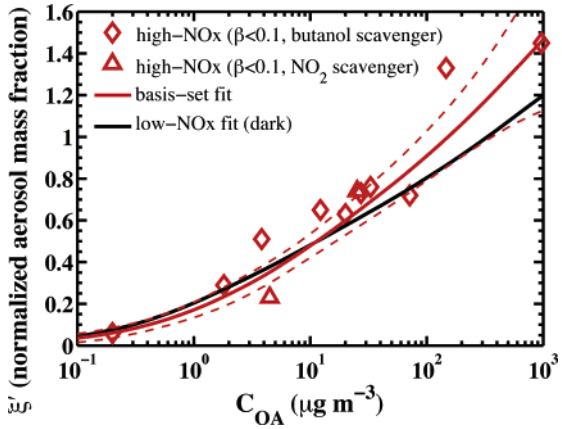

Figure 4. NO_x effect for limonene ozonolysis. All plotted data are ξ' for very high NO_x, with both 2-butanol (◊) and NO_2 (△) serving as the OH scavenger. For comparison, the low-NOx (dark) fit is shown. There is relatively little change in the SOA mass relative to the low-NO_x case, though there appears to be a modest increase in ξ' at high C_{OA}.

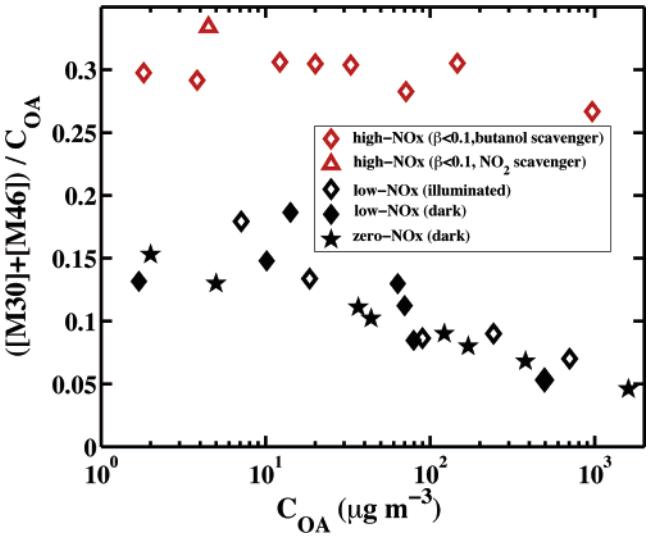

Figure 5. AMS results for the fraction of the SOA mass at masses 30 and 46 as a function of C_{OA}. The black ♦ shows an experiment at very low NO_x (2 ppb) on 1/19/06, and the black ★ are for the NO_x-free experiments conducted in a 100 L Teflon bag.

Whereas α-pinene + O_3 showed a sharp drop in the AMF at high NO_x, limonene + O_3 shows little change, with at most a slight increase in SOA formation at high SOA concentration (>20 μg m^{-3}). We shall discuss this in detail below; however, it appears that there are two competing effects in play, brought into focus because oxidation of both double bonds produces very low vapor pressure products even at high NO_x. First, products in the high-NO_x pathway appear to be somewhat more volatile than their low-NO_x counterparts, as with α-pinene. However, the high-NO_x products include organic nitrates, which add considerable mass (an NO_2 group) to the SOA, increasing the mass yields. In these experiments, high-NO_x (β < 0.1) is maintained until well after completion of SOA formation, so any decrease of NO_x concentration should not influence the data.

We used the AMS to assess organic nitrate formation for limonene. Figure 5 shows the sum of the mass 30 and mass 46 divided by the total aerosol mass as a function of C_{OA} for all the experiments that have AMS data available. AMS data are

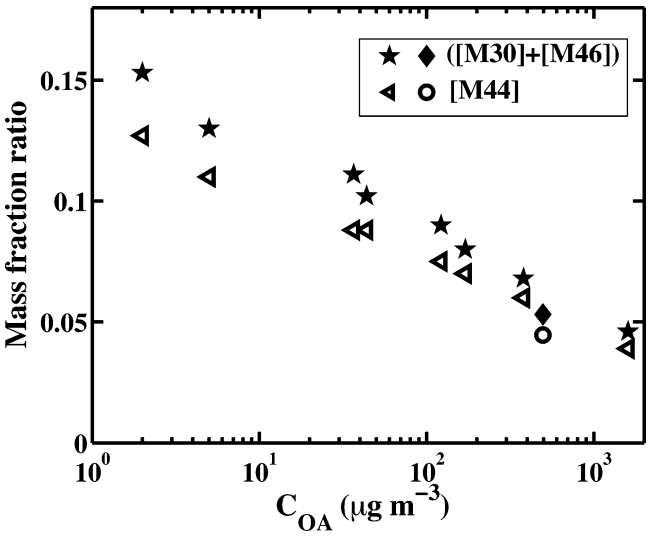

Figure 6. Fraction of the total SOA mass at mass 44 and masses 30 and 46 in NO_x-free experiments, as a function of the total aerosol mass. The results from a very low NO_x experiment in the smog chamber (2 ppb, on 1/19/06) are also shown in ♦ and ○ for comparison. This shows that the nonnitrate contribution to masses 30 and 46 correlates strongly with mass 44 (CO_2^+) and also that the low C_{OA} aerosol (which is less volatile) is relatively more oxygenated.

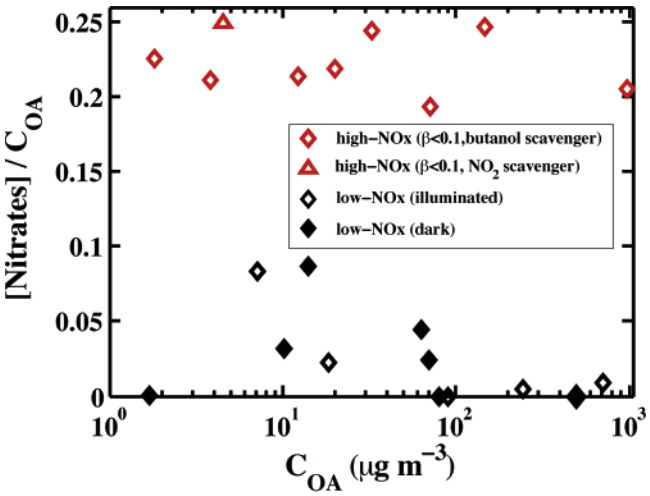

Figure 7. Fraction of the SOA mass attributed to nitrate fragments, after correction for nonnitrate contributions to masses 30 and 46 as a function of the total SOA concentration.

frequently analyzed with a "fragmentation table" designed to approximate ambient conditions,[57] in which mass 46 is completely attributed to the NO_2 group and mass 30 is mostly attributed to the NO group. This approximation is not valid in our experiments.

To evaluate the contribution of the nonnitrate fragments at masses 30 and 46, we performed 8 NO_x-free experiments with 4−6 ppm O_3 in a 100 L Teflon bag with pure nitrogen and oxygen. The data are shown in Figures 5 and 6 with stars. The fraction of the total SOA mass at masses 30 and 46 decreases almost linearly with aerosol concentration on a logarithmic scale. Our challenge is to relate these NO_x-free data to high-NO_x data, realizing that the chemical mechanism is different under these two conditions. We shall rely on a surrogate feature—the mass 44 peak (a CO_2^+ fragment), which is often used as an indicator of oxygenated aerosol.[58] Figure 6 shows the aerosol fraction for mass 44 and for the sum of masses 30 and 46 from the NO_x-free experiments. Both fractions decrease with increasing aerosol concentration, and the ratio of these two indicators is a constant 1.2. A single point (marked with diamond and circle) from a low-NO_x, low-O_3 experiment is shown (with a diamond and circle) in Figure 6 to verify that the correlation between the mass fragments is the same in both the smog chamber and the Teflon bag. The fact that the ozone concentrations are much different in the NO_x-free experiments also indicates that there is no O_3 dependence to the relationship between $m/z = 44$ and 30+46.

The contribution of nitrate represented by masses 30 and 46 to the total aerosol mass is shown in Figure 7, again as a function of the total SOA mass. The nitrate fraction under high-NO_x conditions is nearly constant at 0.22. This confirms that nitrate contributes substantial mass to the SOA; this also confirms that formation of nitrate products under high-NO_x does not change the volatility distribution significantly. The low-NO_x data also contain some nitrates because of the finite VOC:NO_x—some RO_2 reacts with NO in these experiments to produce nitrates. The high nitrate fraction (0.08) for two low-NO_x experiments is caused by both high background NO_x and low limonene, which gives β around 0.5.

In one low-NO_x experiment, 800 ppb of NO and O_3 were added to the chamber 3.5 h after oxidation had been initiated and long after the limonene had been consumed. The UV lights were switched on at the same time. The SOA concentration profile was unchanged, showing that NO_x influences the SOA formation only while the gas-phase chemistry is active, which is similar to UV radiation effect. It also shows that formation of nitric acid will not rapidly catalyze any increased SOA formation after the gas-phase oxidation has reached completion.

4.4. OH Scavenger Effect. The HO_x and O_3 chemistry is substantially more involved at high NO_x. HO_x−NO_x interactions with UV illumination lead to significant O_3 production, which we observe. A dramatic increase in the O_3 concentration is caused by a radical chain reaction initiated by OH radical produced after O_3 addition to limonene. The net reaction is that 2-butanol reacts with O_2 in the presence of UV radiation, forming 2-butanone, H_2O, and O_3. Under these conditions the "HO_x conditioning" of the butanol is compromised, but fortunately NO_2 acts as a true HO_x scavenger whereas NO becomes the major RO_2 sink. The formation of $HONO_2$ from OH and NO_2 is the chain termination reaction; this suggests that the butanol may be unnecessary under high-NO_x conditions. In two high-NO_x experiments, 2-butanol was not used. These data are shown in Figures 4 and 7 with triangles, from which we can see that the absence of 2-butanol has very little influence on the AMF or the nitrate ratio. Both results confirm that neither formation of $HONO_2$ nor the specific HO_x conditioning has a significant influence on aerosol formation in the high-NO_x experiments.

4.5. Lower O_3 Results. The high initial ozone in most of our experiments has the potential to obscure the reaction mechanism by simply making all processes fast. To further constrain the mechanism, we conducted experiments with high limonene and lower O_3. The experimental conditions and results are tabulated in the Supporting Information. Initially, the low-O_3 experiment setup followed the same procedure as the high-O_3 experiments, just with much less initial ozone. After about 3 h, the O_3 concentration was raised by more than an order of magnitude to oxidize any remaining unsaturated compounds.

The results are striking. We present data from representative high- and low-NO_x experiments in Figures 8−10. In the high-NO_x experiment (open red circles toward the bottom of each panel of Figure 8), butanol was not used to keep O_3 as low as possible. Ozone fluctuated during this experiment due to radical

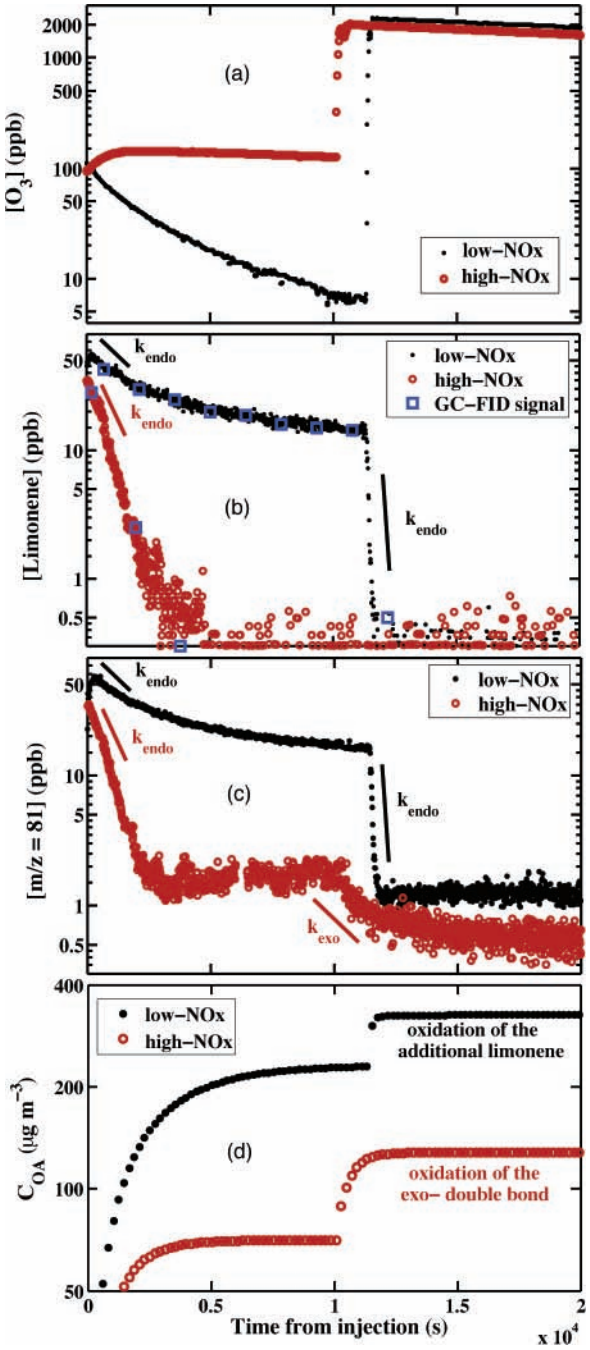

Figure 8. Reduced ozone experiments at low (black) and high (red) NO_x. (a) Ozone concentration, showing photochemical steady-state at high NO_x and steady decline at low NO_x, followed at around 3 h in each case by a large ozone injection. (b) Limonene concentration profile measured by both PTR-MS ($m/z = 137$) and GC-FID (blue □), showing first-order decay of limonene after first O_3 injection. (c) The PTR-MS signal at $m/z = 81$, showing first-order decay of a secondary product at high NO_x after second injection of ozone. (d) The wall-loss corrected SOA concentration profile measured by SMPS.

chain reactions but remained between 85 and 200 ppb, as shown in Figure 8a. In Figure 8b, both the PTR-MS (at $m/z = 137$) and GC-FID data show that in 4000 s essentially all of the limonene was consumed, at which time the normalized AMF was a modest 0.33. The PTR-MS signals at $m/z = 137$ and 81 are consistent in most of the experiments, but they show different behavior in this case. The PTR-MS data at $m/z = 81$ in Figure 8c show a small residual (2 ppb) that is certainly due to a fragment from a limonene oxidation product. The initial lifetime of limonene for this experiment was around 800 s, giving a

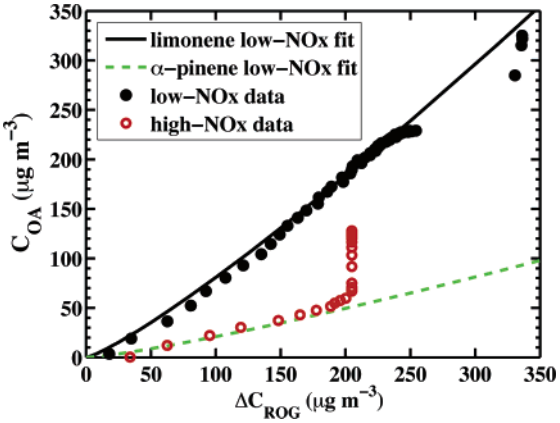

Figure 9. SOA "growth curves" based on PTR-MS and SMPS real-time data for limonene + ozone under low-ozone conditions at low- (black) and high- (red) NO_x conditions for the same two experiments depicted in Figure 8. Growth curves from the basis-set fits for low-NO_x limonene (black line) and low-NO_x α-pinene (green line) are shown for reference. The low-NO_x real-time data fall on the nominal growth curve, showing that the final volatility distribution is produced at the limonene oxidation rate; however, the high-NO_x data show a dramatic "hook" after addition of supplemental ozone, showing a second generation of oxidation that sharply reduces the volatility distribution of the reaction products.

rate constant of 3×10^{-16} cm^3 molecule^{-1} s^{-1} (indicated with a red line labeled "k_{endo}").

The addition of 2 ppm of ozone after 3 h resulted in a gradual decay of the residual mass fragment, revealing a second-order rate constant of 7×10^{-18} cm^3 molecule^{-1} s^{-1} (indicated with a red line labeled "k_{exo}"). This secondary decay is entirely consistent with the expected rate constant for a terminal double bond in the gas phase, indicating that under high-NO_x conditions a significant fraction of the first-generation reaction products (most of which will retain the terminal double bond) remain in the gas phase in the presence of 100 ppb of ozone, with a gas-phase lifetime of 10 h or so. They can, however, be oxidized readily with additional ozone, resulting in a sharp increase in the aerosol mass.

The situation at low NO_x is completely different. In the low-NO_x experiment (filled black circles toward the top of each panel of Figure 8), O_3 was completely consumed after 2 h because there was no photochemical O_3 source inside the bag. The limonene-ozone stoichiometry in this initial phase was roughly 1:2 (initial black data points in Figure 8a,b), indicating that both double bonds in the limonene were being oxidized on a time scale far shorter than the expected gas-phase lifetime of the terminal double bond. When the ozone was depleted, only 70% of the limonene was consumed, but the AMF was substantial at 0.94.

The initial lifetime of limonene for the low-NO_x experiment was about 3000 s, giving a rate constant of 2×10^{-16} cm^3 molecule^{-1} s^{-1}. This is not statistically different from the high-NO_x case, given the imprecision of extracting a second-order rate constant from these data. The second ozone addition after 3 h removed the residual limonene rapidly, consistent with the high endocyclic rate constant (as shown in Figure 8b), leaving only a stable, low, background signal at $m/z = 81$, possibly caused by a saturated, second-generation reaction product. There was no sign of slow oxidation of a terminal double bond, again indicating that this terminal double bond was oxidized more or less simultaneously with the endo- double bond.

After 2 ppm of O_3 was added at approximately 3 h, the aerosol concentration increased quickly in each experiment.

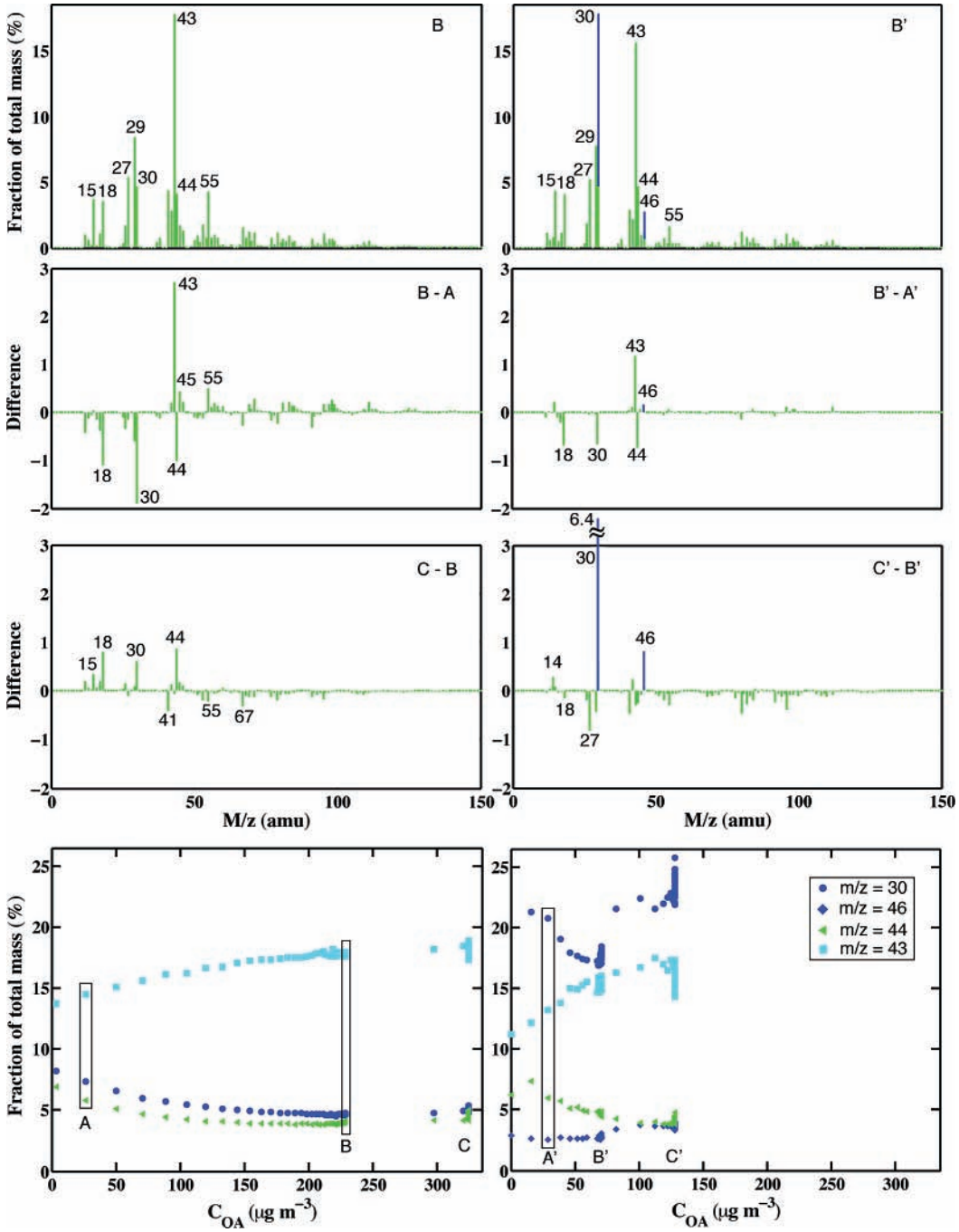

Figure 10. Aerosol mass spectra for low-NO_x and high-NO_x conditions at different reaction times and organic aerosol loadings, plotted as a percentage of the total mass response. The reference spectrum (B) is taken at the end of each low-O_3 period shown in Figure 8—at the gap in the low-NO_x data and the bottom of the sharp hook in the high-NO_x data in Figure 9. Two differences are shown in each case. The first (B−A) compares the reference to AMS spectra early in the experiment at low C_{OA}. The second (C−B) compares the reference to AMS spectra late in the experiment at high C_{OA}. The reference spectra are consistent with limonene ozonolysis, with small alkyl fragments (and little $m/z = 57$ because the major source is $C_4H_9^+$, which is not found in these compounds) and a modest $m/z = 44$ signal from organic acids and hydroperoxides. The high-NO_x spectrum (B′) also reveals nitrate features, shown in blue. The first difference (B−A) in each case shows that the lower C_{OA} spectra (A) are relatively more oxidized, with B−A at $m/z = 18$, 30, and 44 being favored over $m/z = 43$ in the lower C_{OA} case. The second difference (C−B) in the low-NO_x case is relatively small, with the most significant feature being a shift toward smaller mass fragments, suggesting that lower carbon number material is condensing at the highest C_{OA}. The second difference in the high-NO_x case shows a surge in nitrate features, suggesting that relatively volatile nitrates are drawn into the condensed phase by oxidation of the second double bond. Selected masses are plotted vs C_{OA} in the lower panel, which shows the steady evolution under low-NO_x conditions from relatively oxidized material of the lowest volatility (lowest C_{OA}) to relatively reduced material at higher volatility. The high-NO_x data show an enigmatic "ripening" in the major features, with a shift in response at the $m/z = 30$ and 43 peaks after the aerosol mass has stabilized.

However, the reasons were completely different. The AMF increased from 0.33 to 0.61 for the high-NO_x experiment, indicating that the added ozone significantly decreased the volatility of the product mix, although all the limonene was consumed by the first ozone injection. Conversely, the AMF kept nearly constant at 0.95 for the low-NO_x experiment, showing that the volatility distribution of the relatively small 30% residual of limonene left in that experiment when the ozone was consumed was nearly identical to the volatility distribution of the initial products.

The difference between the low- and high- NO_x is vividly apparent on a "growth curve" of the type described by Ng et al.,[16] shown in Figure 9. This shows the observed (normalized) aerosol loading as a function of the precursor loss, measured in real time with the PTR-MS. The figure also shows for reference the asymptotic aerosol growth curves based on basis-set fits for limonene and α-pinene (each with high O_3 and low-NO_x). The low-NO_x, low-O_3 data progress along the asymptotic curve for most of the experiment, with the exception of a few points just after the massive increase of ozone at 3 h (causing a gap between 250 and 325 μg m^{-3}), where condensation kinetics appear to cause the aerosol mass to lag the equilibrium value slightly. This shows unequivocally that under low-NO_x conditions initial oxidation of the endo- double bond is rate limiting, and the reaction products almost immediately show very low volatility, even at low O_3.

The high-NO_x, low-O_3 data in Figure 9 differ markedly from the low-NO_x data, lagging well below the asymptotic curve in real time. After the limonene is completely removed and supplemental ozone is added, the growth curve hooks vertically, showing the unmistakable sign of secondary oxidation leading to lower volatility products. Thus under high-NO_x conditions, oxidation of the exo- double bond is rate limiting. More accurately, the two generations of oxidation are well separated under these conditions. Also, under high-NO_x conditions, the initial AMF (when only one double bond is oxidized) appears to be substantially decreased relative to our "standard" system (low-NO_x limonene + O_3). This is consistent with our earlier findings for α-pinene.[36]

Note that the wall-loss corrected C_{OA} in the second half of the growth curve is a lower limit because our wall-loss correction does not account for aerosol mass residing on the chamber walls; this mass is likely to absorb some of the semivolatile vapors generated in the second oxidation step, reducing the growth of the suspended aerosol. The analysis here depends on the shape of the growth curve (especially the dramatic hook at high NO_x) and not the magnitude of the growth after the second ozone addition.

Differences in the SOA composition are readily apparent in AMS spectra obtained during these low-O_3 experiments and shown in Figure 10. We focus on three periods, labeled A, B, and C (with A′, etc. for the high-NO_x case). The middle period, B, is used as the reference and plotted first because it corresponds to the stable period at the end of the low-O_3 portion of the experiment. The spectra plot the percentage of the total mass at each fragment mass. Two difference spectra are plotted below, revealing the changes in composition during aerosol growth (A−B) and after the large O_3 addition (B−C).

For the low-NO_x data, we note the following. The first difference, A−B, shows that the low C_{OA} aerosol are substantially more oxidized than the higher C_{OA} aerosol, shown by the difference between m/z 30 and 44 vs 43 (note that the m/z = 18 contribution to organics is set equal to the m/z = 44 component in the fragmentation table). This is entirely consistent with highly oxidized compounds that yield m/z = 44 fragments (for instance organic acids) condensing at low C_{OA}. These oxidized compounds are then diluted by more reduced compounds at higher C_{OA}, as partitioning theory would suggest. The second difference is modest, but there is a hint that almost all of the larger fragments are reduced at the end—it may be that the most volatile compounds appearing in the aerosol at the end are systematically smaller, having lost at least one more carbon than their less volatile counterparts. The overall trends in key fragments are shown in the bottom panel as a (linear) function of C_{OA}.

The high-NO_x AMS spectra tell a different story, dominated by nitrates. The first-stage (low O_3) spectra show considerable nitrate contributions at m/z = 30 and 46, plotted in blue in the spectra in the right-hand column of Figure 10. The first difference (B′−A′) again shows that as the aerosol grows reduced fragments gain at the expense of oxidized fragments. However, the large ozone addition draws a very significant portion of additional nitrate into the aerosol, with almost all of the second difference spectrum (C′−B′) being in nitrate features (note that the m/z = 30 difference is off scale). This is consistent with relatively volatile nitrates being drawn into the aerosol after the exo double bond is oxidized.

5. Discussion

5.1. Comparison with Literature Data. The lifetime of limonene in our high-O_3 experiments is 200−300 s, roughly the mixing time scale in our chamber, whereas the lifetime of limonene in our low-O_3 experiments is 1200−2300 s. Under both conditions, we were able to analyze limonene decay observed in the PTR-MS to obtain a first-order rate constant, which we could then scale with the ozone concentration to estimate the bimolecular rate constant (e.g. Figure 8a for low-O_3 conditions). The value was $(2.3 \pm 0.4) \times 10^{-16}$ cm^3 $molecule^{-1}$ s^{-1}. These are crude measures of the kinetics, but they do reveal that the oxidation rate of the limonene itself is entirely consistent with the known gas-phase rate constant for ozone + limonene (2.0×10^{-16} cm^3 $molecule^{-1}$ s^{-1}).[28,29]

The SOA production in our experiments is much greater than that observed by Griffin et al.[3] Nøjgaard et al.[59] addressed the effect of NO_x concentration on particle formation during ozonolysis of α-pinene and limonene, concluding that increasing NO_x decreases the number concentration of aerosol formed from both α-pinene and limonene. This is consistent with our findings as they performed the experiments at low-O_3. Although the aerosol mass fraction increases with increasing NO_x in our high-O_3 experiments, the NO_x concentration has no influence on number concentration of the formed aerosol, and the mode of aerosol formed at high NO_x is usually bigger than that of aerosol formed at low NO_x.

Leungsakul et al. measured SOA formation at very high limonene, relatively low ozone, low-NO_x, dark conditions.[10] Although the temperature varied from 264 to 296 K, the AMF results are consistently about 30% lower than the levels in our low-O_3 experiments. However, the experiments were photooxidations, including both ozone and OH reactions without OH scavengers, and Leungsakul et al. report a maximum aerosol concentration without wall loss correction. The aerosol concentration after wall loss correction in our experiments is usually 15−25% larger than the maximum aerosol concentration, and visual inspection of the data in their paper (Figure 4) shows evidence for a similar wall-loss rate in experiments where most of the limonene was consumed.

5.2. SOA Formation Mechanism. The data shown in Figures 8 and 9 reveal a striking difference between low- and high-NO_x conditions. We believe that this is caused by a dramatic change in the ozonolysis kinetics for the second (exo) double bond in limonene. Specifically, under low-NO_x conditions, the exo double bond is oxidized by heterogeneous uptake of ozone to fresh particles containing unsaturated, first-generation limonene oxidation products, whereas under high-NO_x conditions, the exo double bond is oxidized in the gas phase at a rate commensurate with gas-phase ozonolysis of terminal double bonds.

The evidence for heterogeneous oxidation in the low-NO_x case is indirect but overwhelming. There are two main aspects. First, the very large SOA production ultimately seen from limonene under all conditions clearly requires significant oxidation of both double bonds. Analogous systems with a single endo double bond, such as α-pinene[56] or limonoketone,[24] produce much less SOA (as shown in Figure 2). The 2:1 ozone/limonene stoichiometry revealed in Figure 8 confirms this. Second, the initial ozone−limonene reaction at low NO_x is clearly rate limiting. The limonene decay follows a single exponential, and the growth curve in Figure 9 shows no significant time lag between the dynamic and steady-state SOA production. We have every reason to expect the homogeneous rate constant for the terminal (exo) double bond to be about 25 times slower than the endo rate constant, and this expectation is confirmed in our high-NO_x data; consequently, some faster process must be consuming the exo double bond. The only viable option is heterogeneous oxidation of unsaturated compounds in the condensed phase. When these compounds are oxidized, the less volatile reaction products remain in the condensed phase and the compounds are immediately replaced by condensation from the vapor, the replacements are oxidized, and so forth until essentially all of the unsaturated vapors are "pumped" into the condensed phase by this heterogeneous process.

The high-NO_x data are clearly different, with a two-part growth curve and much slower secondary kinetics. The secondary kinetics occurs at just the rate expected of gas-phase ozonolysis of a terminal double bond, and so there is no reason to believe it is anything else. It is impossible to assess the stoichiometry because of the catalytic ozone production with NO_x and UV illumination, but the secondary reactions more than double the overall aerosol mass (depending on the uncertain wall loss of product vapors, the increase could be a factor of 3−4). These high-NO_x data are thus qualitatively consistent with what we would expect to see for a two-step homogeneous process for doubly unsaturated terpenes.[16,17]

We hypothesize that the heterogeneous uptake coefficient (γ) for ozone on the limonene SOA changes quite dramatically with NO_x levels in our chamber, resulting in one limit where the initial ozonolysis of the endo double bond is rate limiting (thus uptake is faster) and another where the secondary ozonolysis of the exo double bond (which is 25 times slower) is rate limiting. On its face, this would seem to require a change of almost a factor of 100 in γ (or, of course, much more). The question is whether this is reasonable, and the answer is "yes".

We can place limits on the uptake coefficient by considering the switch in rate-limiting behaviors described above. This is depicted in Figure 11, which shows the time scales for homogeneous and heterogeneous processes over the duration of the low- and high-NO_x experiments. We take the gas-phase time scales as known, the endo double bond time scale corresponding to the known rate constant for ozone + limonene and the exo double bond time scale corresponding to the expected terminal double bond rate constant (observed rate of loss observed for the secondary products under high-NO_x conditions). The endo time scale is plotted as a definite horizontal line, whereas we give a range for the exo time scale with a green band spanning a factor of about 2.5, making the exo time scale 10−25 times slower than the endo time scale. For the rate-limiting steps to change as observed, the heterogeneous oxidation time scale must be faster than (below) the gas-phase endo time scale in the first case and slower than (above) the gas-phase exo time scale in the second case. These limits are shown in gray.

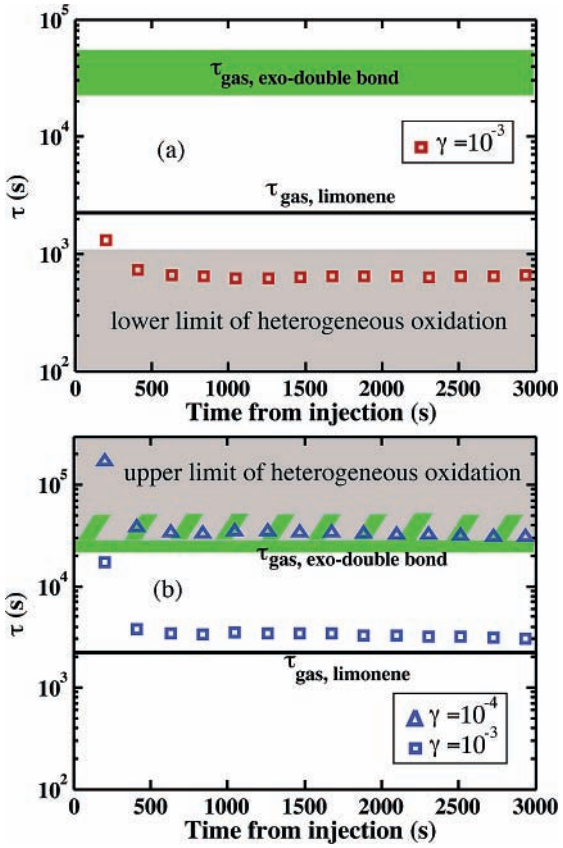

Figure 11. Chemical time scale for both homogeneous and heterogeneous oxidation in limonene ozonolysis. Figures are for low-O_3 (100 ppb) with (a) low NO_x and (b) high NO_x. Homogeneous lifetimes (horizontal line for endo- and green block for exo- double bonds) are for ozone reacting with gas-phase limonene and limonene oxidation products. Heterogeneous lifetimes (□ and △) are for ozone reacting with first-generation products in the condensed phase assuming different uptake coefficient γ. The low-NO_x time-dependent data show rapid processing of the first-generation products (shown in gray), which is consistent only with rapid condensed-phase oxidation ($\gamma e 10^{-3}$). The high-NO_x time-dependent data show slow processing of the first-generation products, which is consistent with gas-phase oxidation. The shadow area in the bottom figure at high-NO_x shows the overlap from gas-phase oxidation of the exo- double bond and the upper limit of the heterogeneous oxidation.

The heterogeneous lifetimes depend on the ozone uptake coefficient γ, the aerosol surface area A_s, and the total mass of organic material to be oxidized, C_{COC}.

$$\tau = \frac{4}{\gamma \bar{c} A_s} \times \frac{C_{COC}}{[O_3]} \qquad (2)$$

where $\bar{c}$ is the mean molecular speed of oxidant at concentration $[O_3]$ in the gas phase. C_{COC} is based on the notion that the complete pool of unsaturated, semi-volatile, first-generation products must be "pumped" out of the vapor and processed in the condensed phase. Most of the condensable material is processed to obtain the observed AMF of order unity. For this calculation, we assume that $C_{COC} = 1.4\Delta C_{limonene}$ for a nominal $C_{10}O_4$ first-generation oxidation product.

The absolute values of γ required for this scenario are very reasonable. The red squares for the low-NO_x case indicate the lifetime $\gamma = 10^{-3}$, which is the uptake coefficient for ozone on pure oleic acid.[19] These are quite consistent with the required

heterogeneous time scale if the reaction of ozone with limonene is to be rate limiting—only for the first few hundred seconds, when the surface area is very small and almost all of the organics are in the vapor phase, would the heterogeneous processing be limiting. The gray area gives a time scale comfortably less than the limonene oxidation time scale; we regard this as a reasonable inference: certainly $\gamma > 5 \times 10^{-4}$ at low-NO_x. The blue triangles show the heterogeneous time scale for high-NO_x conditions given $\gamma = 10^{-4}$, where the heterogeneous time scale would just equal the fastest possible gas-phase time scale for the exo double bond. This is thus very much an upper limit to γ under high-NO_x conditions. The aerosol size distributions for the high- and low- NO_x cases are similar; on average the high-NO_x particles are about 50% larger. We account for this difference and it will not produce the dramatic, multiple order of magnitude effect that we observe.

Combined, these results show that the heterogeneous uptake coefficient for ozone to the first-generation limonene SOA can vary by at least a factor of 5 and quite probably much more with changes in the chemical composition of that SOA. This occurs even though many of the molecules in these high-NO_x particles must be unsaturated. The cause of this effect is unknown, but the magnitude is entirely reasonable. Recent work has shown that the heterogeneous oxidation of oleic acid on atmospheric particles[60] and even laboratory mixtures[22,61] is much slower than for pure particles, implying that γ is reduced by up to a factor of 1000 in the ambient case.[60] It is possible that phase changes play a role,[22] but we have evidence that the low-NO_x SOA from limonene + ozone is in the condensed phase, at least for relatively low C_{OA} [Kostenidou, personal communication], so it is not obvious that this could be the cause. It is also possible that the ozone + alkene rate constants themselves are changed in the particles due to solvent effects. The causes of the rate reduction remain uncertain, but the results shown here suggest that composition can have a major effect.

At least one fact remains something of a puzzle. Oxidizing one endocyclic double bond in α-pinene under low- and high-NO_x conditions renders products with very different volatility distributions whereas oxidizing both double bonds in limonene renders products under either condition with very similar volatility distributions. There is strong evidence that condensed-phase chemistry is important to the overall volatility distribution,[10] and we can speculate that the reaction product distributions from the full oxidation of limonene, even under high-NO_x conditions, favor oligomer formation, whereas for some still unknown reason, the products generated after oxidation of only a single endo- double bond by ozone in the presence of NO_x are not so favorable. It is also quite possible that heterogeneous oxidation occurs for a brief period under high-NO_x conditions, only to be shut down after only a portion of the vapors are "pumped" into the condensed phase.

This begs the question of what happens to limonene in the atmosphere. We know that ozone uptake coefficients appear to be reduced for almost all condensed-phase compounds in realistic model mixtures,[61] and so we can speculate that the heterogeneous processing we see here under low-NO_x conditions may be much slower in the atmosphere. It is far more difficult to anticipate what the vapor pressure distribution of the second-generation products will be when that oxidation occurs in the gas phase. The evidence from our high-NO_x experiments suggests that those gas-phase secondary products will also have a much lower vapor-pressure distribution than the first-generation products, on average, but that conversion from first to second generation will occur rather slowly. Indeed, for terminal double bonds, OH and ozone are competitive oxidants.

6. Conclusions

The limonene-ozone system does indeed serve as an outstanding model system for multiple-generation oxidation of organic aerosol precursors. Under a range of conditions, including low- and high- NO_x, dark and UV-illuminated, and relatively low and high ozone levels, we see more than a factor of 3 variation in the organic aerosol mass fractions. Although the high-NO_x oxidation products from α-pinene + ozone have significantly higher vapor pressures than the low-NO_x α-pinene + ozone products, those two pathways appear to yield products with similar vapor pressure distributions for limonene. However, NO_x influences the kinetics strongly. Specifically, heterogeneous oxidation of the first-generation products by ozone uptake on unsaturated SOA particles drives a large fraction of the total mass into the condensed phase at low NO_x, but this heterogeneous pathway is much slower at high NO_x, leaving gas-phase ozonolysis to form the high-NO_x second-generation products. These sensitivities to NO_x suggest that great care must be exercised in extrapolating laboratory results for these systems to the atmosphere.

Several important questions remain unanswered. First, the factors behind the changes to the heterogeneous uptake coefficient are unknown, and they may well be the key to understanding ozone uptake on atmospheric particles. Second, because we do not know the appropriate uptake coefficient for atmospheric particles, we cannot constrain specific product yields for atmospheric modeling. However, these results certainly confirm the potential for limonene to be a very important source of biogenic SOA. Third, we have explored only the first two generations of oxidation at the two unsaturations in limonene. Those second-generation products will be subject to continued oxidation by OH radicals and continued photolysis, and we know that this will continue to alter the volatility distribution.[15] However, we do not know how far this oxidation can proceed toward lower volatility; full oxidation produces CO_2, so eventually carbon−carbon bond cleavage will dominate the reactions and the aerosol will evaporate. This may well begin to dominate at O:C of 1:1 or so, meaning that the second-generation oxidation products observed here may be near the lower limit of the volatility distribution possible from a C_{10} precursor.

Acknowledgment. This work was supported by grants RD-83108101 from the US EPA and ATM-0446495 from NSF. Although the research described in this manuscript has been funded in part by the United States Environmental Protection Agency, it has not been subjected to the Agency's required peer and policy review and therefore does not necessarily reflect the views of the Agency and no official endorsement should be inferred.

Supporting Information Available: Complete data tables for the experiments discussed in this paper as well as figures showing the effect of UV illumination at various points during an experiment. This material is available free of charge via the Internet at http://pubs.acs.org.

References and Notes

(1) Singh, H. B.; Salas, L.; Viezee, W.; Ferek, R. *Atmos. Environ. Part A* **1992**, *26*, 2929.

(2) Guenther, A. et al. *J. Geophys. Res.* **1995**, *100*, 8873.

(3) Griffin, R. J.; R., C. I. D.; Seinfeld, J. H. *Geophys. Res. Lett.* **1999**, *26*, 2721.

(4) Guenther, A.; Geron, C.; Pierce, T.; Lamb, T.; Harley, P.; Fall, R. *Atmos. Environ.* **2000**, *34*, 2205.

(5) Bernhard, C. A.; Kirchner, S.; Knutti, R.; Lagoudi, A. In *Proceedings of Healthy Buildings '95*; Proceedings of the Fourth International Conference on Healthy Buildings; Maroni, M., Ed.; Milan, Italy, 1995.

(6) Brown, S. K.; Sim, M. R.; Abramson, M. J.; Gray, C. N. *Indoor Air* **1994**, *4*, 123.

(7) Clausen, P. A.; Wilkins, C. K.; Wolkoff, P.; Nielsen, G. D. *Environ. Int.* **2001**, *26*, 511.

(8) Girman, J. R.; Hadwen, G. E.; Burton, L. E.; Womble, S. E.; McCarthy, J. F. In *Proc. Indoor Air '99* **1999**, *2*, 460.

(9) Wolkoff, P.; Clausen, P. A.; Wilkins, C. K.; Nielsen, G. D. *Indoor Air* **2000**, *10*, 82.

(10) Leungsakul, S.; Jaoui, M.; Kamens, R. M. *Environ. Sci. Technol.* **2005**, *39*, 9583.

(11) Jay, K.; Stieglitz, L. *Product Analysis of the Chemical/Photochemical Conversion of Monoterpenes with Air Pollution and Ecosystems*; Proceedings of Air Pollution and Ecosystems; Grenoble, France, 1987.

(12) Calogirou, A.; Larsen, B. R.; Kotzias, D. *Atmos. Environ.* **1999**, *33*, 1423.

(13) Glasius, M.; Lahaniati, M.; Calogirou, A.; Jensen, N. R.; Hjorth, J.; Kotzias, D.; Larsen, B. R. *Environ. Sci. Technol.* **2000**, *34*, 1001.

(14) Donahue, N. M.; Huff Hartz, K. E.; Chuong, B.; Presto, A. A.; Stanier, C. O.; Rosenφrn, T.; Robinson, A. L.; Pandis, S. N. *Faraday Discuss.* **2005**, *130*, 295.

(15) Donahue, N. M.; Robinson, A. L.; Stanier, C. O.; Pandis, S. N. *Environ. Sci. Technol.* **2006**, *40*, 2635.

(16) Ng, N. L.; Kroll, J. H.; Keywood, M. D.; Bahreini, R.; Varutbangkul, V.; Flagan, R. C.; Seinfeld, J. H.; Lee, A.; Goldstein, A. H. *Environ. Sci. Technol.* **2006**, *40*, 2283.

(17) Kroll, J. H.; Ng, N. L.; Murphy, S. M.; Flagan, R. C.; Seinfeld, J. H. *Environ. Sci. Technol.* **2006**, *40*, 1869−1877.

(18) Rudich, Y. *Chem. Rev.* **2003**, *103*, 5097−5124.

(19) Rudich, Y.; Donahue, N. M.; Mentel, T. F. *Annu. Rev. Phys. Chem.* Submitted.

(20) Robinson, A. L.; Donahue, N. M.; Rogge, W. F. *J. Geophys. Res.* **2006**, *11*, D03302 DOI: 10.1029/2005JD006265.

(21) Knopf, D. A.; Anthony, L. M.; Bertram, A. K. *J. Phys. Chem. A* **2005**, *109*, 5579−5589.

(22) Katrib, Y.; Biskos, G.; Buseck, P.; Davidovits, P.; Jayne, J.; Mochid, M.; Wise, M.; Worsnop, D.; Martin, S. T. *J. Phys. Chem. A* **2006**, *109*, 10910.

(23) Zhang, J.; Dransfield, T. J.; Donahue, N. M. *J. Phys. Chem. A* **2004**, *108*, 9082.

(24) Tischuk, J.; Marquis, B.; Huff Hartz, K. E.; Zhang, J.; Donahue, N. M. *J. Am. Chem. Soc.* **2006**, Submitted.

(25) Huff Hartz, K. E.; Donahue, N. M.; Pandis, S. N. *Environ. Sci. Technol.* **2006**, in Preparation.

(26) Criegee, R. *Angew. Chem., Int. Ed. Engl.* **1975**, *14*, 745.

(27) Atkinson, R.; Hasegawa, D.; Aschmann, S. M. *Int. J. Chem. Kinet.* **1990**, *22*, 871.

(28) Shu, Y.; Atkinson, R. *Int. J. Chem. Kinet.* **1994**, *26*, 1193.

(29) Calvert, J. G.; Atkinson, R.; Kerr, J. A.; Madronich, S.; Moortgat, G. K.; Wallington, T. J.; Yarwood, G. *The Mechanisms of Atmospheric Oxidation of the Alkenes*; Oxford University Press: New York, 2000.

(30) Atkinson, R.; Baulch, D. L.; Cox, R. A.; Crowley, J. N.; Hampson, R. F.; Kerr, J. A.; Rossi, M. J.; Troe, J. *Summary of Evaluated Kinetic and Photochemical Data for Atmospheric Chemistry*; Technical Report, IUPAC Subcommittee on Gas Kinetic Data Evaluation for Atmospheric Chemistry, 2002 (http://www.iupac-kinetic.ch.cam.ac.uk/).

(31) Fenske, J. D.; Hasson, A. S.; Ho, A. W.; Paulson, S. E. *J. Phys. Chem. A* **2000**, *104*, 9921.

(32) Greene, C. R.; Atkinson, R. *Int. J. Chem. Kinet.* **1992**, *24*, 803.

(33) Pankow, J. *Atmos. Environ.* **1994**, *28*, 185.

(34) Pankow, J. *Atmos. Environ.* **1994**, *28*, 189.

(35) Odum, J.; Hoffmann, T.; Bowman, F.; Collins, D.; Flagan, R.; Seinfeld, J. *Environ. Sci. Technol.* **1996**, *30*, 2580.

(36) Presto, A. A.; Hartz, K. E. H.; Donahue, N. M. *Environ. Sci. Technol.* **2005**, *39*, 7036.

(37) Shrivastava, M. K.; Lipsky, E. M.; Stanier, C. O.; Robinson, A. L. *Environ. Sci. Technol.* **2006**, *40*, 2671.

(38) Tolocka, M. P.; Jang, M.; Ginter, J. M.; Cox, F. J.; Kamens, R. M.; Johnston, M. V. *Environ. Sci. Technol.* **2004**, *38*, 1428.

(39) Seinfeld, J. H.; Pandis, S. N. *Atmospheric Chemistry and Physics: From Air Pollution to Climate Change*; John Wiley & Sons: New York, 1998.

(40) Baugues, K. *A Review of NMOC, NO_x, and NOMC/NO_x ratios measured in 1984 and 1985*; U. S. Environmental Protection Agency report EPA-450/4-86-015: Research Triangle Park, NC, 1986.

(41) National Research Council *Rethinking the Ozone Problem in Urban and Regional Air Pollution*; National Academy Press: Washington, DC, 1991.

(42) Thompson, A. M.; Johnson, J. E.; Torres, A. L.; Bates, T. S.; Kelly, K. C.; Atlas, E.; Greenberg, J. P.; Donahue, N. M.; Yvon, S. A.; Saltzman, E. S.; Heikes, B. G.; Mosher, B. W.; Shashkov, A. A.; Yegorov, V. I. *J. Geophys. Res.* **1993**, *97*, 16955.

(43) Pandis, S. N.; Paulson, S.; Seinfeld, J.; Flagan, R. *Atmos. Environ. Part A* **1991**, *25*, 997.

(44) Kwok, E. S. C.; Aschmann, S. M.; Atkinson, R.; Arey, J. *Faraday Trans.* **1997**, *93*, 2847.

(45) Presto, A. A.; Hartz, K. E. H.; Donahue, N. M. *Environ. Sci. Technol.* **2005**, *39*, 7045.

(46) Song, X.; Polissar, A. V.; Hopke, P. K. *Atmos. Environ.* **2001**, *35*, 5277.

(47) Takahama, S.; Wittig, A. E.; Vayenas, D. V.; Davidson, C. I.; Pandis, S. N. *J. Geophys. Res.* **2004**, *109*, D16S06.

(48) Kim, E.; Hopke, P. K.; Kenski, D. M.; Koerber, M. *Environ. Sci. Technol.* **2005**, *39*, 4953.

(49) Atkinson, R.; Aschmann, S. M.; Winer, A. M. *J. Atmos. Chem.* **1987**, *5*, 91.

(50) Carter, W. P. L.; Atkinson, R. *J. Atmos. Chem.* **1989**, *8*, 165.

(51) Stanier, C. O.; Pandis, S. N. *Environ. Sci. Technol.* **2006**, in press.

(52) Huff Hartz, K. E.; Rosenφrn, T.; Ferchak, S. R.; Raymond, T. M.; Bilde, M.; Donahue, N. M.; Pandis, S. N. *J. Geophys. Res.* **2005**, *110*, D14208.

(53) Chew, A. A.; Atkinson, R. *J. Geophys. Res.* **1996**, *101*, 28649.

(54) Keywood, M.; Kroll, J.; Varutbangkul, V.; Bahreini, R.; Flagan, R.; Seinfeld, J. *Environ. Sci. Technol.* **2004**, *38*, 3343.

(55) Pathak, R. K.; Stanier, C. O.; Donahue, N. M.; Pandis, S. N. *J. Geophys. Res.* Submitted.

(56) Presto, A. A.; Donahue, N. M. *Environ. Sci. Technol.* **2006**, *40*, 3536−3543.

(57) Allen, J. D.; Limenez, J. L.; Williams, P. I.; Alfarra, M. A. Bower, K. N.; Jayne, J. T.; Coe, H.; Worsnop, D. R. *J. Geophys. Res.* **2003**, *108*, 4090, DOI: 10.1029/2002JD002358.

(58) Zhang, Q.; Worsnop, D. R.; Canagaratna, M. R.; Jimenez, J. L. *Atmos. Chem. Phys.* **2005**, *5*, 3289.

(59) Nøjgaard, J. K.; Bilde, M.; Stenby, C.; Nielsen, O. J.; Wolkoff, P. *Atmos. Environ.* **2006**, in press.

(60) Robinson, A. L.; Donahue, N. M.; Rogge, W. F. *J. Geophys. Res.* **2006**, *11*, D03302 DOI: 10.1029/2005JD006265.

(61) Huff Hartz, K. E.; Weitkamp, E.; Sage, A. M.; Donahue, N. M.; Robinson, A. L. *J. Geophys. Res.* Submitted.